Open Access Full Text Article

ORIGINAL RESEARCH

Electroacupuncture Alleviates Lung Injury in CpG1826-Challenged Mice via Modulating CD39-NLRP3 Pathway

Jiasi Wu [iD], Xin Xiong, Xiumin Hu

Acupuncture and Tuina School, Chengdu University of Traditional Chinese Medicine, Chengdu, Sichuan, People's Republic of China

Correspondence: Jiasi Wu, Email wujiasi@cdutcm.edu.cn

Purpose: Cytokine storm secondary lung injury (CSSLI) is the leading death cause in COVID-19 virus infection, and CD39-dominated purinergic brake drives NLRP3 inflammasome activation and pyroptosis, which plays a crucial role in the pathogenesis of CSSLI. Though electroacupuncture (EA) can alleviate lung injury caused by a variety of inducers, its effect on CSSLI and the underlying mechanism needs further investigation.

Methods: We established a widely recognized CSSLI mice model with CpG1826 (CpG), a TLR-9 agonist agent. Luminex liquid chip was employed to detect serum levels of 12 cytokines/chemokines to evaluate cytokine storm formation. H+E staining and transmission electron microscope were applied to examine pulmonary pathological injury and alveolar macrophage structure, respectively. IL-1β, IL-18, IL-1α, and HMGB-1 in BAL fluid were determined by ELISA kits. mRNA and protein levels of lung CD39 and NLRP3 were assessed by qRT-PCR and Western blotting. An in vitro model was also established by incubating PMA-differentiated THP-1 cells with serum samples obtained from relevant group of mice.

Results: Repeated CpG induced CSSLI together with the elevation of 11 cytokines/chemokines including GM-CSF, IL-16, IL-1α, MCP-1, IL-2, IL-10, CCL3, IL-1β, TNF-α, IL-6, and IL-17A, though not IFN-γ, which was reduced by EA pretreatment to a different extent. EA also alleviated lung injury and recovered lung macrophage structure. Moreover, CpG enhanced IL-1β and IL-18 level in BAL fluid, promoted NLRP3, while suppressing CD39 expression in lung, all of which were reversed by EA pretreatment. Of note, EA failed to further decrease BAL fluid IL-1β, IL-18, IL-1α, and HMGB-1 levels when A438079, a selective inhibitor of P2X7, was administered. However, both CD39 and NLRP3 are dispensable for EA decreasing multi-cytokine secretion in serum-incubated and CpG-stimulated THP-1 cells. Taken together, EA alleviated CSSLI in CpG-challenged mice by regulating the CD39-NLRP3 pathway in a P2X7-dependent way.

Conclusion: EA demonstrated potential to be applied in COVID-19 treatment.

Keywords: electroacupuncture, cytokine storm, CD39, NLRP3 inflammasome, lung injury, CpG1826

Introduction

The term "cytokine storm" was first described in 1993, and the unexpected outbreak of COVID-19 worldwide made it a heated research hotspot in the recent three years.[1] Excessive production of cytokines like interleukin, chemokines, and interferons is believed to be a hallmark of COVID-19, which aggravates pulmonary dysfunction and failure.[2,3] Indeed, cytokines get involved in diverse pro-inflammatory reactions via enhancing pathogen detection and the homeostasis of immune cells, macrophages in particular.[4] Cytokine storm secondary lung injury (CSSLI) is characterized by abnormal immune activation resulting from excessive macrophage activation, and it has been one of the leading death causes of COVID-19 infection.[5] Though the combination use of antibiotics and (or) monoclonal antibody demonstrates a certain ameliorative effect, the high financial burden and unavoidable adverse reaction superposition make it an urgent need to reveal the underlying pathogenesis of CSSLI and explore novel, accessible, and cost-effective alternative therapeutic means.

3245

Pyroptosis occurring in pulmonary macrophages plays a crucial role in acute lung injury, and this process can be principally triggered by inflammasome activation.[6] Inflammasomes are intracellular platforms containing cytosolic pattern recognition receptors, among which nucleotide-binding oligomerization domain-like receptor pyrin domain containing 3 (NLRP3) is the most in-depth studied and clinically implicated one.[7,8] Purinergic CD39 functions as hydrolyzing ATP, the accumulation of which mediates NLRP3 activation and further controls the maturation of IL-1β and IL-18.[9] Therefore, modulating the CD39-NLRP3 pathway may be beneficial in CSSLI.

With a small electric current passing between a pair of acupuncture needles, electroacupuncture (EA) is a form of acupuncture, which is a widely recognized traditional Chinese medicine documented in ancient medical books like *The Yellow Emperor's Classic of Internal Medicine*.[10] In recent years, the anti-inflammatory effect of EA has been announced in China and abroad. For example, Torres-Rosas et al reported that EA suppressed inflammatory response in septic mice via acting like a selective dopamine agonist.[11] More precisely, low-intensity EA at hindlimb regions (Zusanli, ST36) could drive the vagal-adrenal axis to further potentiate anti-inflammatory effects that depend on NPY+ adrenal chromaffin cells.[12] However, whether and how EA alleviates CSSLI remains unclear.

In the present study, we conducted repeated TLR-9 stimulation by its ligand cytosine guanine dinucleotide [CpG]-oligodeoxynucleotide 1826 to establish a mouse model of macrophage activation syndrome to mimic CSSLI, and hypothesized that low-intensity EA at ST36 could alleviate CSSLI by modulating the CD39-NLRP3 pathway.

Materials and Methods

Animals and Experimental Design

A total of 48 male C57BL/6 mice aged 6–8 weeks were purchased from Sichuan Academy of Medical Sciences (Chengdu, China) and adaptively fed for one week before scheduled to experiments. All experimental protocols were under the guidance of the recommendations of the *Ministry of Science and Technology of China's Guidance for the Care and Use of Laboratory Animals*, and were approved by the Animal Care and Use Committee of Chengdu University of Traditional Chinese Medicine (license number: SYXK [Chuan] 2014–124; ethical approval number: 2020–21). All mice were housed and provided free access to food and water at a temperature of 23–25 °C as well as a humidity of 45–55%, and were maintained on a 12/12 h light/dark cycle.

Mice were randomly divided into four groups labeled as Control, CpG only, CpG+EA, and CpG+Sham. Mice in the CpG group received repeated CpG injections, those in CpG+EA group were treated with 5 doses of CpG (50 μg) over the course of 10 days followed by EA treatment as previously reported with minor modification.[13,14] Mice in CpG+Sham group only received acupuncture needles without any electrical stimulation. Mice in CpG+Sham group were also challenged with repeated CpG while only received acupuncture needles without any electrical stimulation.

Electroacupuncture Pretreatment

EA intervention in present study refers to previous studies with minor modification.[11,12,15] In brief, pretreatment with EA was performed at Zusanli (ST36) acupoint 0.5 h before each CpG administration by applying EA instruments (No. SDZ-IIB, Suzhou Medical Appliances). Briefly, animals from all groups were anesthetized by inhaled isoflurane (0.5–1.5%) via a precision vaporizer and then laced on a heating pad in order to maintain body temperature. The location of acupuncture points is determined referring to '*the Atlas of Acupuncture Points in Animals*' formulated by the *Experimental Acupuncture Branch of the Chinese Acupuncture and Moxibustion Society*. Specifically, ST36 is located in the posterolateral knee joint, about 2 mm below the small head of the fibula. Disposable needles (size 0.25×13 mm) were applied for acupuncture, and the depth of acupuncture is about 2–3 mm to the muscle layer. EA was performed with a continuous-mode stimulation for another 15 min, with an electrical current of 3.0 mA, and a frequency of 10 Hz by using a stimulator at the hindlimb ST36 acupoint. The auxiliary needle is located on the mouse at the junction of the right side of the tail and the fur, and it was fixed and electrified slightly beneath the skin. Moreover, mice in the control group not only were anesthetized as well, but also received the repeated injection of the solvent of CpG. All mice were sacrificed 12 h after the last CpG administration as shown in Figure 1. Samples of serum, BAL fluid, as well as lung tissue were collected.
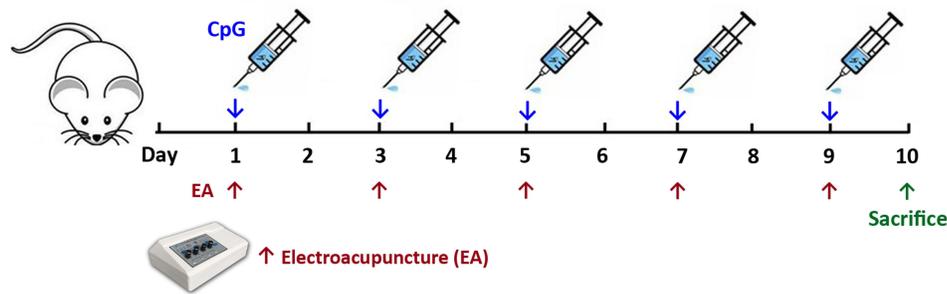
Figure 1 Mice were administered with 5 doses of CpG (50 µg) over the course of 10 days; EA pretreatment at a frequency of 3 mA/10 Hz was performed at Zusanli (ST36) acupoint 0.5 h before each CpG administration.

Luminex Liquid Chip Assay

As previously defined,[16] serum samples from each group were scheduled to high-sensitivity Luminex liquid chip assay for the detection of GM-CSF, IL-16, IL-1α, MCP-1, IFN-γ, IL-2, IL-10, CCL3, IL-1β, TNF-α, IL-6, and IL-17A (*RnD, LXSAMSM-07*), following the standard operation procedure and manufacturer's instructions.

Hematoxylin-Eosin (H+E) Staining of Lung Tissue

Following the sacrifice of all mice on day 10, the right upper lung tissues were excised and then fixed with 4% paraformaldehyde for 48 h. After that, samples were embedded in paraffin before cutting into 5-µm sections, which were further stained with hematoxylin and eosin for observation with Panoramic section scanner (PANNORAMIC150, 3DHISTECH, Hungary). The degree of lung injury was assessed by evaluating interstitial/alveolar edema, hemorrhage, alveolar septal thickening, and infiltration of inflammatory cells as previously described.[17]

Lung Wet (W)/Dry (D) Ratio Measurement

Mice right upper lung was also examined to detect lung W/D ratio. In brief, tissues were firstly weighed to gain the data of wet weight, after which tissues were dried in an oven at temperature of 60 °C for another 1 week to obtain dry weight data. W/D ratio was calculated by dividing those data of the wet weight by the dry wet.

Detection of IL-1β and IL-18 Level in BAL Fluid

BAL fluid was collected following the method reported previously with minor modification.[18] Levels of IL-1β and IL-18 in BAL fluid were examined by using ELISA kits following the manufacturer's protocol (Multi-Science, China).

Transmission Electron Microscopy (TEM)

Fresh lung tissues were removed and washed with PBS, and immediately placed in TEM fixative prepared in advance, in which they were cut into 1 mm^3 pieces. After that, slices were transferred to EP tubes containing glutaraldehyde for 24 h, and were then washed with 0.1M PB (pH 7.4) 3 times. During this process, lung tissue was maintained away from light and was fixed with 1% OsO_4 in PB for 2 h at room temperature. Following the removal of OsO_4, lung tissue was rinsed for a total of three times with PB and was then dehydrated at room temperature. All embedded samples with resin were moved to a 65 °C oven for polymerization over 48 hours. The copper mesh was observed and photographed under a transmission electron microscope.

Western Blotting

Lung tissues were washed with PBS on ice and lysed with RIPA buffer containing PMSF. The separated protein samples were then transferred onto a polyvinylidene difluoride (PVDF) immobilon-P membrane utilizing a transblot apparatus. After 1.5 h at room temperature in TBST containing 5% BSA, membranes were incubated overnight at 4 °C with CD39, NLRP3, and GAPDH primary antibodies. The membranes were washed and then incubated for another 2 h at room temperature with secondary antibodies. The multicolor prestained protein ladder was supplied by Shanghai Epizyme

Biomedical Technology Co., Ltd (Catalogue number WJ103). The signal was detected by enhanced chemiluminescence which was then quantified using Image J software.

Quantitative Real-Time PCR

Following treatment, total RNA was isolated by using a rapid RNA extraction kit referring to the manufacturer's directions and was then reverse-transcribed using the PrimeScript™ RT Reagent Kit (Takara Bio, Shiga, Japan). Equal amounts of cDNA were subjected to quantitative real-time PCR with the fluorescent dye SYBR Green I (Beyotime Biotechnology, Shanghai, China). The primer pairs for NLRP3, CD39, and β-actin were as follows:

NLRP3-F, 5′-TCACAACTCGCCCAAGGAGGA A-3′, *NLRP3-R*, 5′-AAGAGACCACGGCAGAAGCTAG-3′, *CD39-F*, 5′-CTGATTCCTGGGAGCACAT-3′, *CD39-R*, 5′-GACATAGGTGGAGTGGGAGAG-3′, and *β-actin-F*, 5′-CATGAAGTGTGACGTGGACATC-3′, *β-actin-R*, 5′-CAGGAGGAGCAATGATCTTGATC-3′.

The $2^{-\Delta\Delta Ct}$ method was employed to determine the relative fold changes, and the average ΔCT values were normalized to that of β-actin; all samples were evaluated in triplicate.

Establishment of in-vitro CpG-Induced THP-1 Cell Model

Human monocytes THP-1 were purchased from Procell Life Science & Technology (Wuhan, China) and cultured in RPMI-1640 medium supplemented with 10% fetal bovine serum and 1% penicillin-streptomycin. THP-1 monocytes were differentiated by PMA (100 nM, 24 h). A certain amount of serum was collected following EA treatment and was added to PMA-differentiated THP-1 cells at a ratio of 10% 12 h prior to CpG (1 μg/mL) stimulation for another 24 h. During this process, A438079 (30 μM), POM-1 (10 μM), and MCC950 (10 μM) were also added at the same time point as serum, respectively. After that, cell culture supernatant was scheduled for ELISA detection.

Data Analysis and Statistics

All statistical analyses were performed using the *GraphPad Prism* 8 software. Multiple comparisons were performed by one-way ANOVA followed by Bonferroni post-hoc analyses or one-way analysis of variance followed by Tukey's multiple comparison test. The results of at least three independent experiments are expressed as the mean±SEM, and the significance of differences is indicated as (*) $P < 0.05$ and (**) $P < 0.01$.

Results
EA Pretreatment Calms CpG-Elicited Cytokine Storm in Mice

Serum levels of multiple cytokines were assessed by conducting Luminex. As presented in Figure 2, CpG challenge led to overproduction of GM-CSF, IL-16, IL-1α, MCP-1, IL-2, IL-10, CCL3, IL-1β, TNF-α, IL-6, and IL-17A (Figure 2A–D and F–L), but not IFN-γ (Figure 2E, *$P < 0.05$, $n=6$). Compared with CpG group, mice that received EA pretreatment prior to CpG had a significant reduction in IL-16, IL-1α, MCP-1, IL-2, IL-10, IL-1β, and IL-6 (**$P < 0.01$, $n=6$), as well as GM-CSF, CCL3, TNF-α, and IL-17A (*$P < 0.05$, $n=6$). However, Sham EA pretreatment also displayed an inhibitory effect on secretion of IL-16, IL-1α, MCP-1, IL-2, IL-10, CCL3, IL-1β, TNF-α, IL-6, and IL-17A to different extent, only weaker than EA pretreatment. These results suggested pretreatment with EA calms cytokine storm mediated by CpG in mice.

EA Pretreatment Alleviated CpG-Induced Lung Edema and Alleviated Lung Injury

As shown in Figure 3A, H+E staining demonstrated that CpG induced moderate thickening of alveolar wall, mild dilation of alveolar accompanied by neutrophil infiltration, as well as necrosis of a large number of bronchial epithelial cells and increased mucus secretion, all of which were averted by pretreatment with EA. Meanwhile, the pathological score of lung injury in CpG+EA group was significantly decreased compared with that in CpG group (**$P < 0.01$, $n=6$, Figure 3B). Consistent with H+E staining results, stimulation with CpG caused pulmonary edema with elevated W/D ratio which was potently reduced following EA pretreatment (**$P < 0.01$, $n=6$), as shown in Figure 3C, suggesting EA was effective to suppress lung edema and prevent the progress of lung injury induced by CpG.
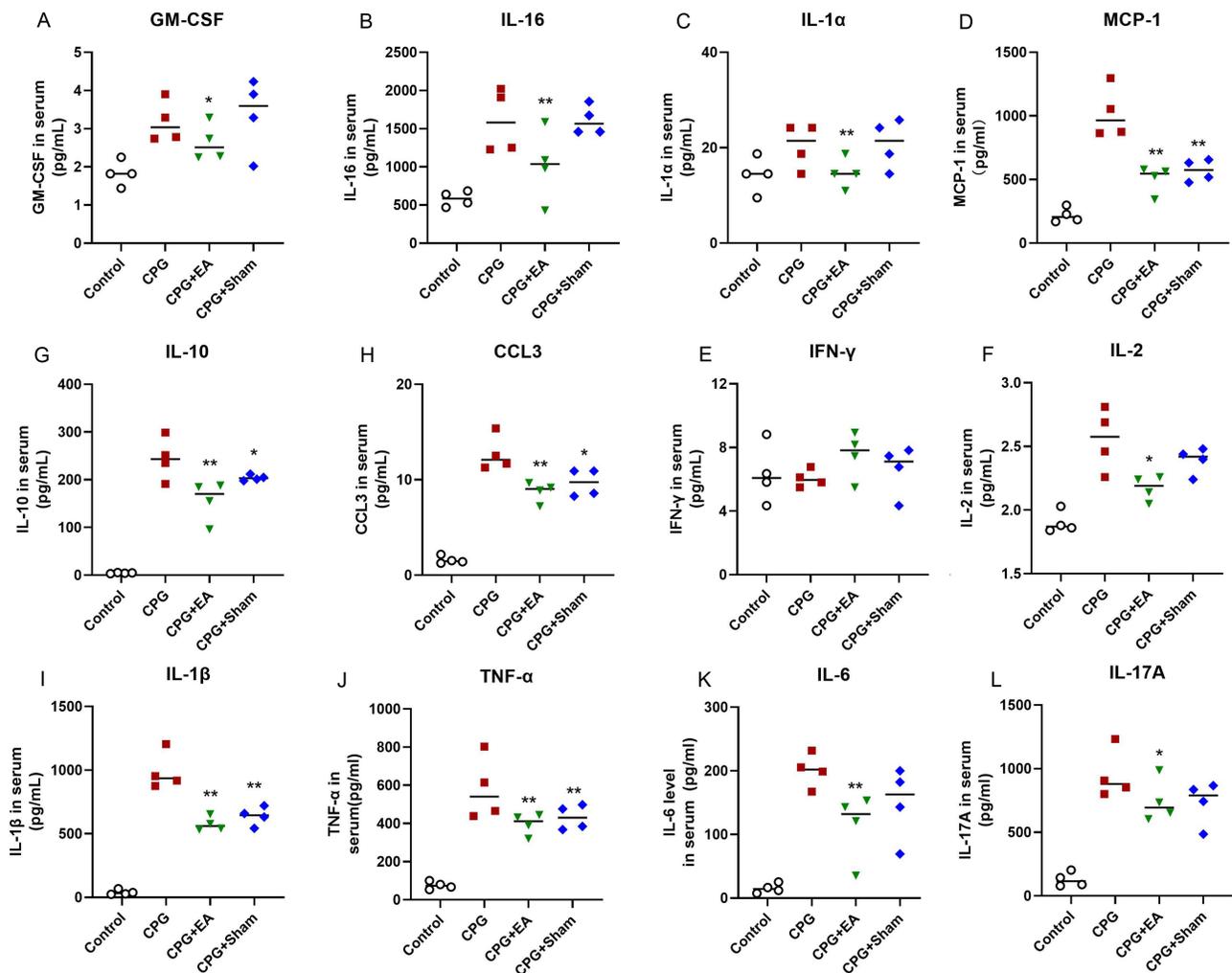
Figure 2 EA pretreatment calms CpG-elicited cytokine storm in mice. Serum levels of (**A**) GM-CSF, (**B**) IL-16, (**C**) IL-1α, (**D**) MCP-1, (**E**) IFN-γ, (**F**) IL-2, (**G**) IL-10, (**H**) CCL3, (**I**) IL-1β, (**J**) TNF-α, (**K**) IL-6 and (**L**) IL-17A were examined by Luminex liquid clip. *$P < 0.05$ and **$P < 0.01$ compared to the CpG group ($n=6$). Data are analyzed using one-way ANOVA followed by Bonferroni post-hoc analyses and are representative of three independent experiments.

EA Pretreatment Recovered Pulmonary Macrophage Structure

As presented in Figure 4, mitochondrial swelling, elevated counts of lysosomes, as well as discontinuous cell membrane were observed in the pulmonary macrophages of the CpG group compared with the control group. However, EA treatment prior to CpG challenge restored the morphology and structures of macrophages, attenuating the degree of mitochondrial swelling and autophagy. These results showed that CpG induced pathological alteration in pulmonary macrophages, while EA pretreatment effectively restrained the destruction of pulmonary macrophage structure, which suggested that EA was able to prevent the development of programmed cell death induced by CpG.

EA Pretreatment Decreased IL-1β and IL-18 Release in Lung

TEM results indicated that EA treatment prior to CpG challenge interfered with the progress of programmed cell death in pulmonary macrophages. To ascertain the specific involved programmed cell death, ELISA kits were used to detect IL-1β and IL-18 concentration in BAL fluid, both of which were key indicators of pyroptotic cell death. As shown in Figure 5A–D, repeated stimulation of CpG resulted in the release of IL-1β and IL-18 in lung, while EA pretreatment but not Sham EA considerably downregulated IL-1β and IL-18 levels in BAL fluid (**$P <0.01$, $n=6$), which suggested that EA pretreatment could diminish IL-1β and IL-18 release into the serum and BAL fluid to further reduce the pyroptotic cell death of pulmonary macrophages.
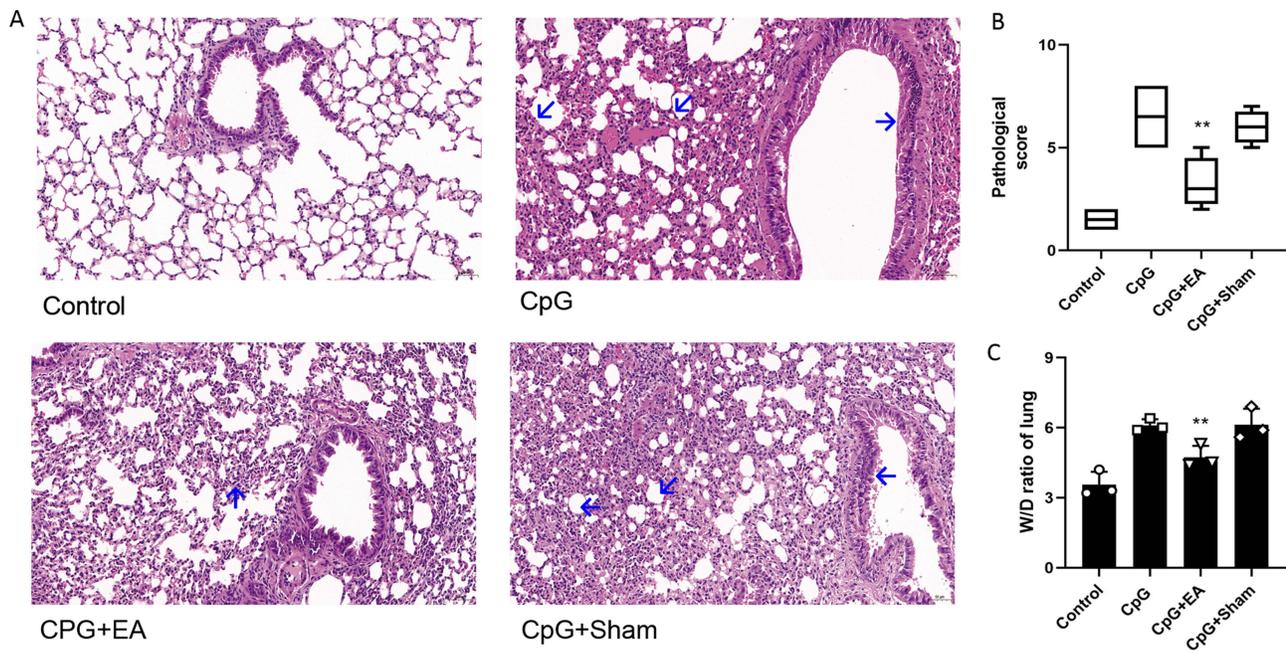
Figure 3 EA pretreatment reversed CpG-induced lung edema and alleviated lung injury. (**A**) H+E staining assessing lung injury induced by CpG. (**B**) Pathological score of lung injury. (**C**) The W/D ratio of the lung. **P < 0.01 compared to the CpG group (*n*=6). Data are analyzed by using one-way analysis of variance followed by Tukey's multiple comparison test and are representative of three independent experiments.
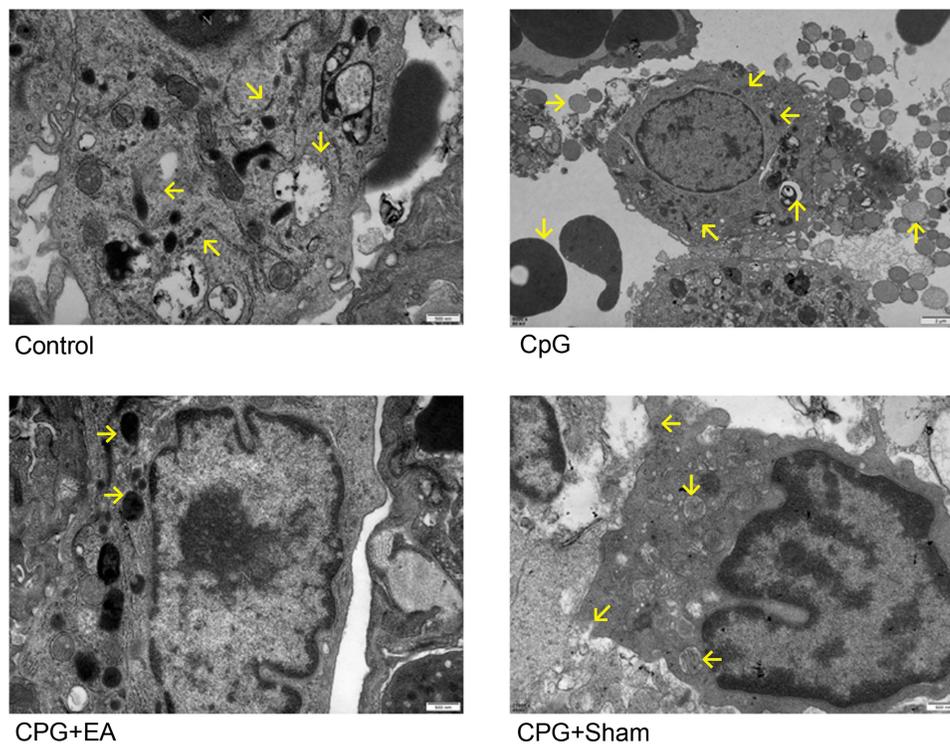

Figure 4 EA pretreatment recovered pulmonary macrophage structure and meanwhile attenuated the degree of mitochondrial swelling and autophagy (marked with yellow arrows). Comparisons between means were carried out using one-way analysis of variance followed by Tukey's multiple comparison test.

EA Pretreatment Inhibited NLRP3 Expression and Enhanced Upstream CD39

NLRP3 inflammasome assembly is one of the key processes that triggers downstream pyroptosis, and purinergic modulator CD39 gets involved in NLRP3 inflammasome regulation. As presented in Figure 6A, mice receiving repeated
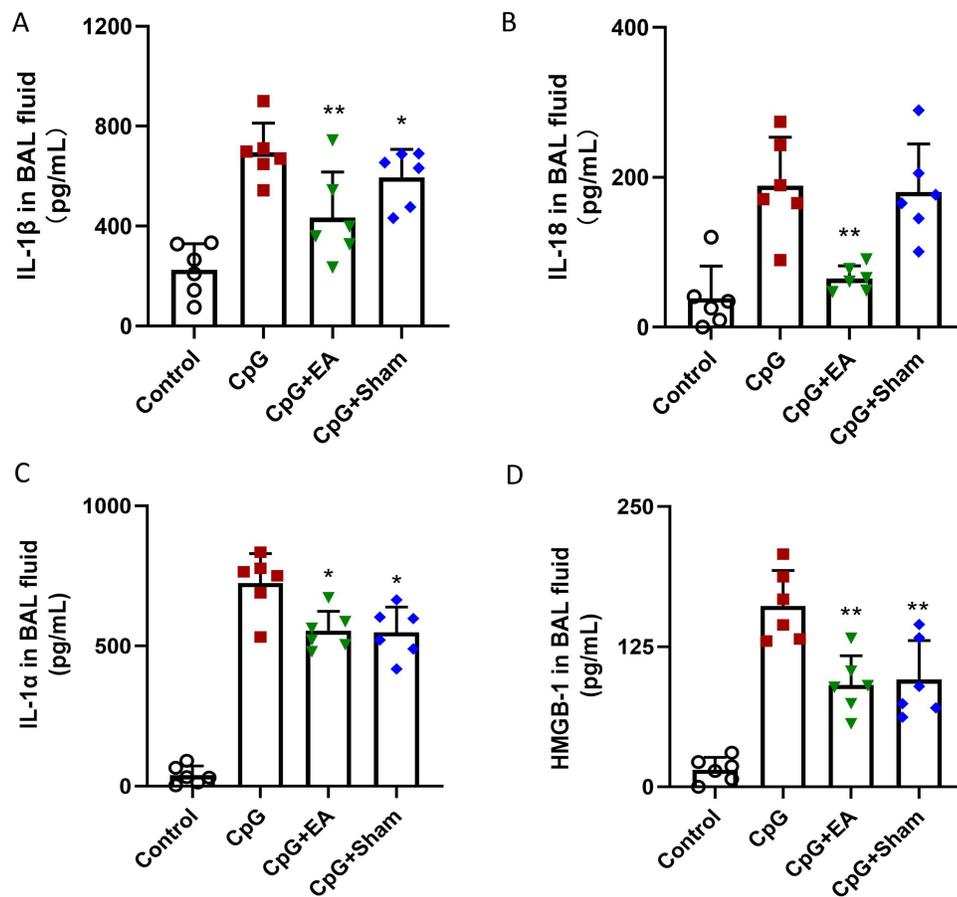
Figure 5 EA pretreatment decreased (**A**) IL-1β, (**B**) IL-18, (**C**) IL-1α and (**D**) HMGB-1 levels in BAL fluid. *P < 0.05 and **P < 0.01 compared to the CpG group (n=6). Data are analyzed using one-way ANOVA followed by Bonferroni post-hoc analyses and are representative of three independent experiments.

CpG injection demonstrated suppressed lung CD39 protein expression. However, both EA pretreatment and Sham EA significantly promoted CD39 protein level (**P <0.01, n=3). In contrast, the enhanced NLRP3 protein expression induced by CpG was potently reduced by EA pretreatment (**P <0.01, n=3) while slightly reduced by Sham EA (*P <0.05, n=3), shown in Figure 6B. To further examine whether EA could regulate mRNA level of NLRP3 and CD39, qRT-PCR was employed, and, consistent with the alterations at protein level, EA promoted CD39 mRNA expression while restraining NLRP3 mRNA expression (Figure 6C and D). These results suggested that EA prevented CpG-induced pulmonary macrophage pyroptosis via modulating the CD39-NLRP3 pathway.

The Ameliorative Effect of EA Pretreatment on CSSLI Was P2X7-Dependent

The dysfunction of CD39 results in accumulation of ATP, which binds to P2X7 to further trigger NLRP3 inflammasome activation. To examine the role played by CD39 in the process of EA improving CSSLI, mice were administered with A438079, the selective antagonist of P2X7 before EA pretreatment and CpG challenge. As shown in Figure 7, blockage of P2X7 by A438079, as well as EA pretreatment both demonstrated suppressive effect on IL-1β (Figure 7A and 7E), IL-18 (Figure 7B and 7F), IL-1α (Figure 7C and (7G), and HMGB-1 (Figure 7D and 7H) contents in BAL fluid and cell culture supernatant. However, with combination application of A438079 and EA (or EA serum), EA failed to further reduce IL-1β, IL-18, IL-1α, and HMGB-1, which suggested that the ameliorative effect of EA on CSSLI through decreasing lung IL-1β, IL-18, IL-1α, and HMGB-1 level was P2X7-dependent (**P <0.01, *P <0.05, n=3).

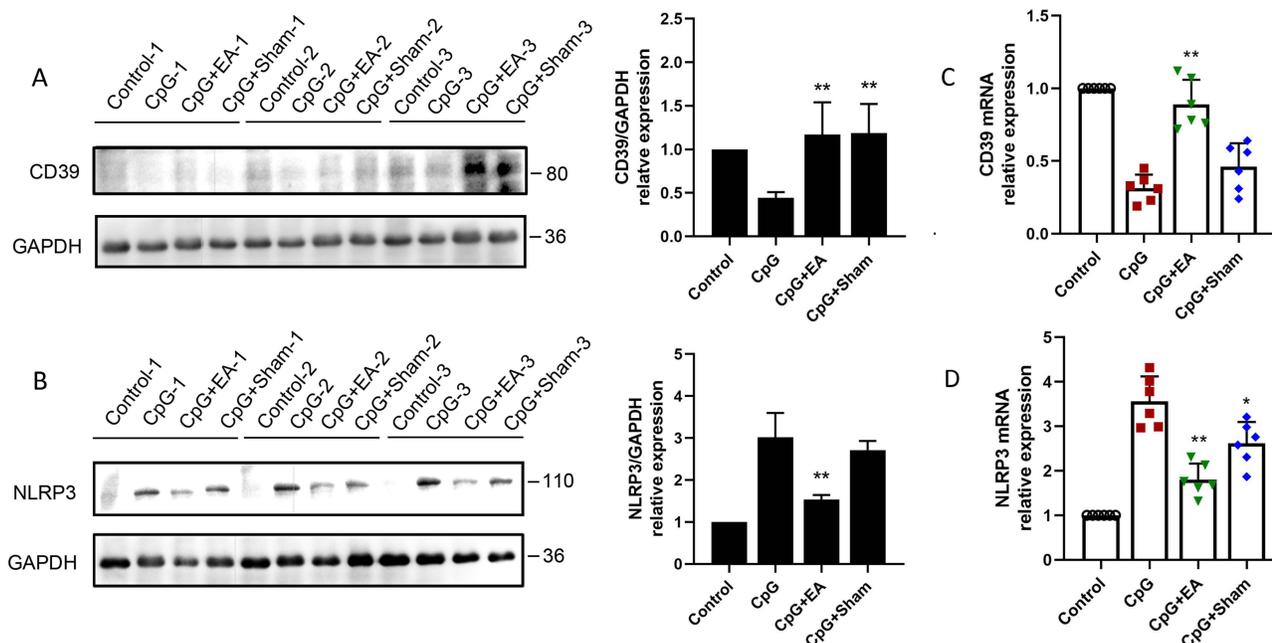**Figure 6** EA pretreatment enhanced (**A**) CD39 protein expression, and inhibited (**B**) downstream NLRP3, via promoting CD39 mRNA expression (**C**), while decreasing NLRP3 mRNA expression (**D**), respectively. *$P < 0.05$ and **$P < 0.01$ compared to the CpG group ($n=3$). Data are representative of three independent experiments.

CD39 and NLRP3 are Dispensable for EA Serum Pretreatment Decreasing Multi-Cytokine Secretion

Similarly, we then evaluated the role played by CD39 and NLRP3 in EA serum pretreatment decreasing multi-cytokine secretion. As shown in Figure 8A–D, blockage of CD39 by POM-1 caused overproduction of IL-1β, IL-18, IL-1α, and HMGB-1, which were all reversed by EA serum pretreatment (*$P <0.05$, $n=3$). In contrast, inhibition of NLRP3 by MCC950 intervention alone significantly reduced the level of the above 4 cytokines. However, different from A438079 which failed to further decrease cytokines level with EA serum supplement, the combination of MCC950 with EA serum pretreatment demonstrated superimposed inhibitory effect, suggesting both CD39 and NLRP3 are dispensable for EA serum pretreatment decreasing multi-cytokine secretion (Figure 8E–H, *$P <0.05$, $n=3$).

Discussion

Accumulative evidence emerging in recent years shows the repeated stimulation of CpG, a well-known TLR-9 agonist, as a reliable method to establish a mice model of macrophage activation syndrome, which involves the formation of cytokine storm.[19,20] In the present study we conducted experiments to assess the effect of EA on cytokine storm secondary lung injury. In fact, repeated CpG stimulation induced cytokine storm formation in mice, which is systemic inflammation. After that, elevated cytokine levels in circulation further mediated multi-organ injury including lung damage. (1) Liu et al announced 3-mA EA pretreatment at ST36 attenuated vagal efferent-independent ongoing systemic inflammation triggered by LPS, another widely recognized inducer of cytokine storm, via driving spinal-sympathetic axis,[12] suggesting EA at ST36 could calm cytokine storm in the early stage and further prevent the progress of lung injury. (2) Besides, a range of research released in recent years indicated that EA at ST36 was capable of rescuing lung injury. For example, EA at ST36 recovered lung function and alleviated both lung and systemic inflammatory response in a mouse model of COPD by regulating dopamine D2 pathway.[21] Preconditioning EA at ST36 could also promote ACE2 expression to improve lung injury in LPS-induced septic rats.[22] Taken together, pretreatment EA at ST36 (3 mA) modulated the spinal-sympathetic axis to attenuate vagal efferent-independent ongoing systemic inflammation (cytokine storm) and prevented the development of secondary lung injury.
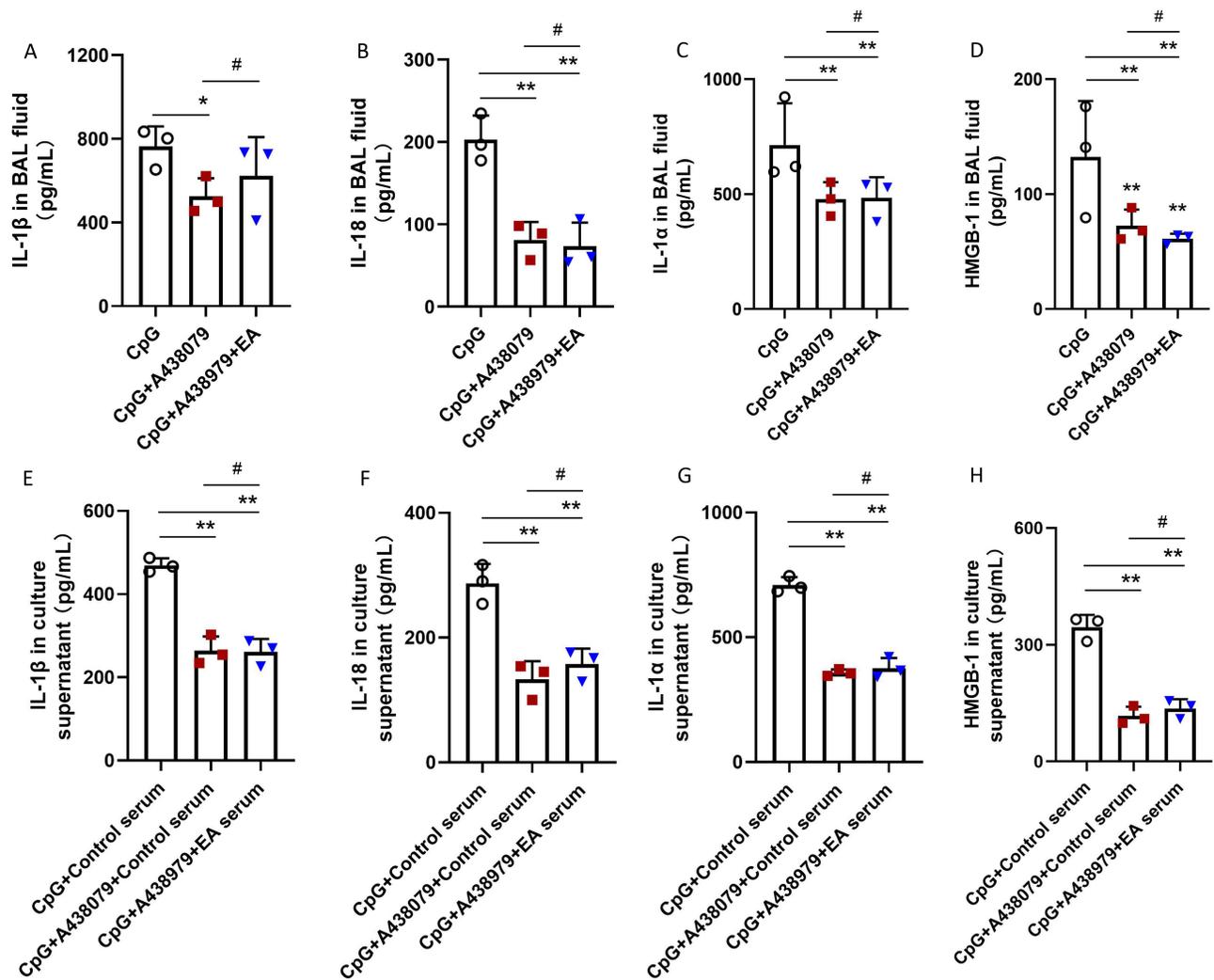
Figure 7 Blockage of P2X7 with A438079 decreased (**A** and **E**) IL-1β, (**B** and **F**) IL-18, (**C** and **G**) IL-1α, and (**D** and **H**) HMGB-1 level in BAL fluid or culture supernatant, while combination use with EA failed to further reduce the amounts of all the above 4 cytokines. **P < 0.01 and *P < 0.05 compared to the CpG group. #no significance (n=3). Data are analyzed using one-way ANOVA followed by Bonferroni post-hoc analyses.

By detecting multi-cytokines, a total of five doses of CpG during a 10-day period drove the mass secretion of GM-CSF, IL-16, IL-1α, MCP-1, IL-2, IL-10, CCL3, IL-1β, TNF-α, IL-6, and IL-17A as expected, and EA treatment prior to CpG stimulation calmed cytokine storm by decreasing all the above 9 cytokines to different extents. Clinical practice indicates that circulatory cytokine storm-facilitated acute respiratory distress syndrome is the leading death cause of COVID-19 infection. Thus, we then evaluated the acute lung injury in CpG-induced mice. Following CpG administration, a range of alterations were observed; those alterations included lung edema, moderate thickening of alveolar wall, mild dilation of alveolar accompanied by neutrophil infiltration, as well as necrosis of a large number of bronchial epithelial cells and increased mucus secretion. Similar with the research of Huang's group in which EA attenuated pulmonary histopathological injury, protein infiltration, and lung water content in rats after cardiopulmonary bypass,[23] EA pretreatment was observed to alleviate CpG-induced lung edema and alleviated lung injury in our study.

Previous study has shown that ultrastructure damage can be observed in cytokine storm secondary lung injury as reported in an LPS-challenged murine model,[24] which is also widely regarded as an animal model of cytokine storm.[25–27] However, it is still unknown whether repeated CpG administration is capable of inducing similar alterations at ultrastructure level as LPS stimulation. In this study, we assessed ultrastructure of lung tissue following CpG treatment by employing TEM, and found that unexpected mitochondrial swelling, boosted lysosome counts, together with
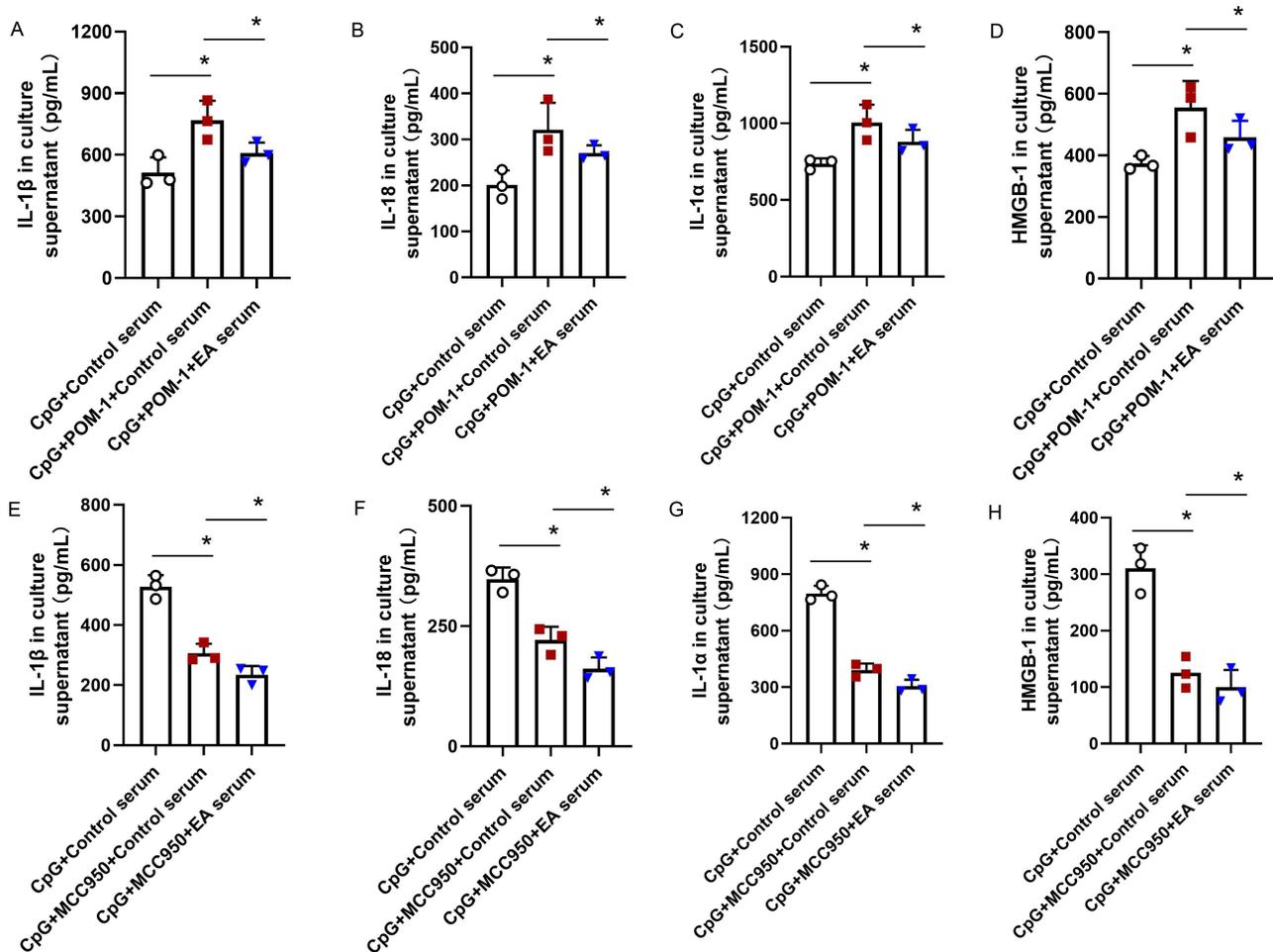
Figure 8 Blockage of CD39 with POM-1 and of NLRP3 with MCC950, respectively, enhanced and reduced the release of (**A** and **E**) IL-1β, (**B** and **F**) IL-18, (**C** and **G**) IL-1α, and (**D** and **H**) HMGB-1 in CpG-stimulated THP-1 cells. However, the effect of EA serum was not blocked after POM-1 and MCC950 incubation. *$P < 0.05$ compared to the CpG group (*n*=3). Data are analyzed using one-way ANOVA followed by Bonferroni post-hoc analyses.

discontinuous cell membrane occurred in alveolar macrophages in response to repeated CpG challenge. However, EA pretreatment played a protective role to reverse ultrastructure change. Indeed, discontinuous cell membrane of alveolar macrophages suggested the involvement of certain programmed cell death during the process of CpG-induced CSSLI. Thus, it will be of interest to further determine the precise type of programmed cell death which occurred in this model, and, on the other hand, it will be meaningful to reveal the exact molecular mechanism of EA pretreatment.

The typically mentioned types of programmed cell death include pyroptosis, apoptosis, autophagy, necrosis, ferroptosis, and cuproptosis, etc, among which pyroptosis is the most relevant one with inflammatory response.[28–30] CD39 is constitutively expressed by various cells of the immune system, and the representative ones include mature B cells, monocytes/macrophages as well as in subsets of CD4, NK cells, and CD8 lymphocytes. Besides, CD39 is also present on epidermal dendritic cells, in which it protects the host from skin inflammatory injury.[31] NLRP3 is mainly distributed in cytoplasm and membrane of immune cells like macrophages and monocytes, and it participates in a variety of host immune and inflammatory responses.[32] Mechanically, reduced CD39 allows the accumulation of ATP which triggers the activation of NLRP3 inflammasome and the following enzymatic autoactivation of caspase-1, after which caspase-1 cleaves pro-IL-1β and pro-IL-18 into their activated form. GSDMD, the representative indicator of pyroptosis, which is also a substrate of caspase-1, and its escaped N-terminal fragment, subsequently localizes and oligomerizes within the plasma membrane to form a pore, providing an exit for bioactive IL-1β and IL-18.[33] Pyroptotic cell death of pulmonary macrophages is one of the key pathological mechanisms of LPS- and cardiopulmonary bypass (CPB)-induced acute lung

injury,[6,34] both of which could be alleviated by EA administration.[35] Therefore, we evaluate the effect of EA pretreatment on the release of IL-1β and IL-18 in lung tissue of CpG-challenged mice. As expected, we observed the inhibitory effect of EA on IL-1β and IL-18 in BAL fluid. Since IL-1β and IL-18 are the direct downstream modulators of pyroptosis, our results indicated that administration of EA displays a certain ameliorative effect via preventing pyroptotic death of lung cells in not only LPS- and CPB-induced, but also repeated CpG-induced acute lung injury, which provides extra support for the clinical application of EA in the fight against pyroptosis-involved acute respiratory distress syndrome. Nevertheless, the underlying mechanism of how EA suppressed IL-1β and IL-18 secretion in lung in CpG-challenged mice remains unclear. To address this issue, we detected the mRNA and protein expression of NLRP3 and its upstream regulator CD39 to verify the inhibitory effect of EA on NLRP3 inflammasome activation. In the present study, we confirmed EA restrained pyroptosis occurring in alveolar macrophages by interfering with NLRP3 inflammasome activation, at least partly through enhancing CD39 expression while suppressing NLRP3 expression.

The dysfunction of CD39 results in accumulation of ATP, which binds to P2X7 to further trigger NLRP3 inflammasome activation. To ascertain the role played by P2X7 in the process of EA ameliorating CSSLI, P2X7's selective antagonist, A438079, was applied before EA or EA serum pretreatment and CpG challenge. Unfortunately, EA failed to further reduce IL-1β, IL-18, IL-1α, and HMGB-1, both in vivo and in vitro, on the basis of A43807's suppression, suggesting the ameliorative effect of EA on CSSLI through diminishing lung IL-1β, IL-18, IL-1α, and HMGB-1 was P2X7-dependent. Given the fact that multiple molecules and pathways could be modulated by EA pretreatment and the suppressive effect of EA on CpG-mediated NLRP3 inflammasome activation was only one aspect of its protective role, future investigation concerning the other route of EA rescuing CpG-caused lung injury is still desperately needed.

It is worth mentioning that pretreatment of EA and Sham EA both showed certain effect among almost all the assessed factors in our study, with more potent effect observed in the EA group than in the Sham EA group. It is actually not uncommon that no statistically significant difference is found between real EA and sham EA in many cases of clinical practice.[36,37] Concerning the basic research, we searched the database again and found that in some cases of EA investigations the sham group also received acupuncture treatment at the same acupoints without electrical current, and meanwhile Sham EA demonstrated similar effect with EA (but much weaker) like the findings observed in our present study. For example, in an animal model of pT-ION-induced nociceptive abnormalities, EA significantly promoted orofacial response threshold while Sham EA showed slight enhancing effect. EA obviously decreased duration of wiping while Sham EA slightly reduced it;[38] Yen et al reported that in the mice medial prefrontal cortex (mPFC), EA and Sham EA significantly and slightly downregulated p-ERK and p-JNK level, respectively, and in the mice periaqueductal gray, EA and Sham EA significantly and slightly enhanced TRPV1 and pPKA level, respectively.[39]

According to Xu et al's research published in the top journal, the *BMJ*,[40] some improper settings have been used on sham acupuncture groups during the last decade, such as selecting adjacent points of the same ganglion segment as stimulation points in the sham group, or using invasive acupuncture needles. These will have the consequence that the intervention of the sham acupuncture group also exerts a certain intensity of acupuncture effect, making it difficult to compare the specificity of the curative effect of the meridian points. A study analyzed the current situation of sham acupuncture control settings in animal experiments, and announced that there is no golden standard yet.[41] In fact, the main methods are application of non-acupoints or acupoints without electrical current. Thus, how to standardize a non-acupoint selecting method and to set an acupuncture standard operation procedure are urgent issues in future investigations.

To sum up (Figure 9), EA pretreatment calms cytokine storm induced by repeat stimulation of CpG in mice, and it ameliorates CSSLI by restraining pyroptosis which occurs in alveolar macrophages via reducing diverse cytokine release through enhancing CD39 expression while inhibiting NLRP3 expression. The suppressive effect is P2X7-dependent but CD39- and NLRP3-independent. Therefore, EA pretreatment can be an alternative clinical therapeutic scenario in the fight against CSSLI like sepsis-induced acute lung injury.
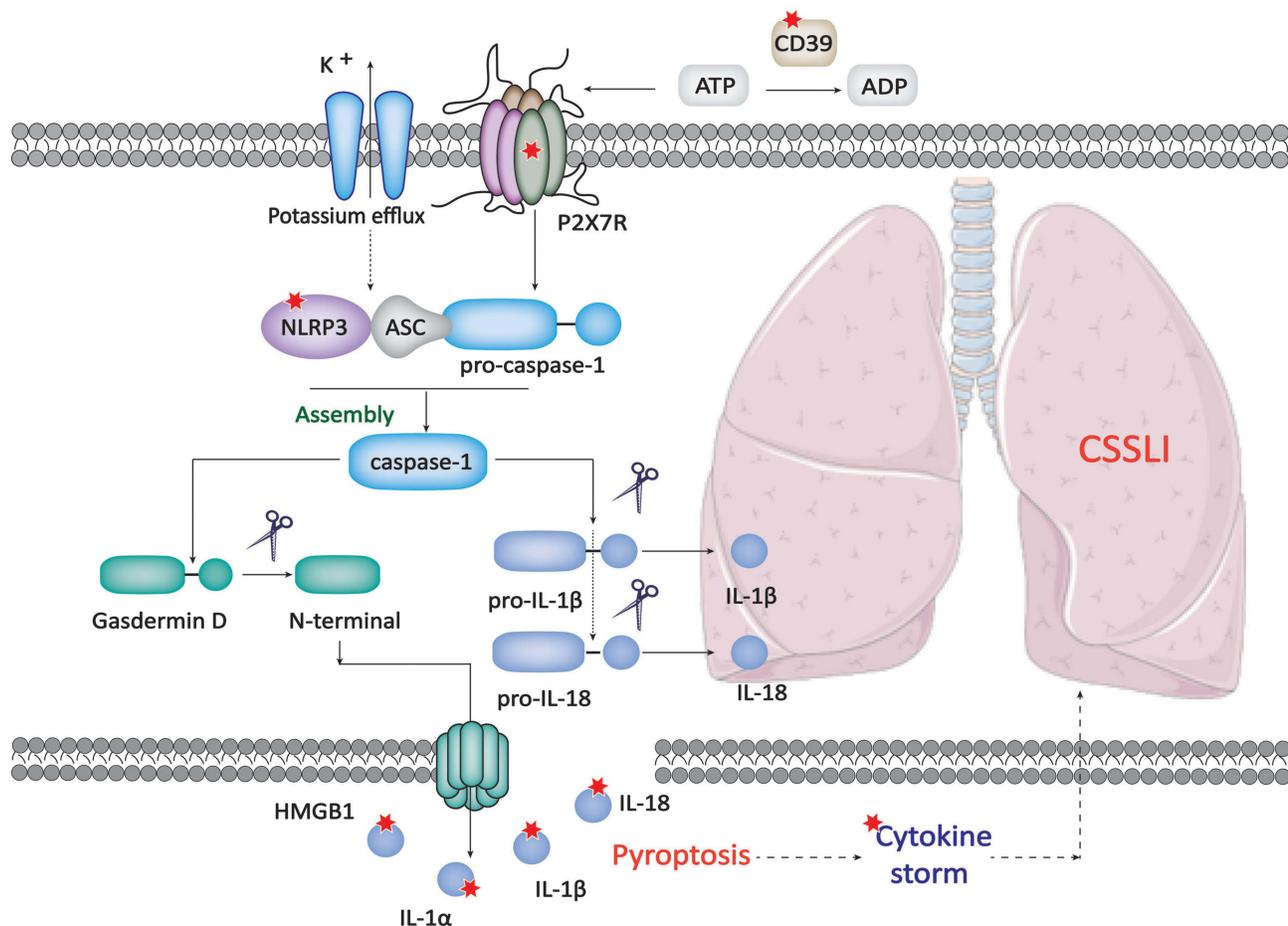
Figure 9 The principal molecular mechanism of how EA pretreatment ameliorates CSSLI. The red star mark represents the verified direct targets of EA.

Abbreviations

CSSLI, cytokine storm secondary lung injury; NLRP3, pyrin domain-containing 3; EA, electropuncture; IL, interleukin; HMGB-1, high mobility group box-1 protein; BAL, bronchoalveolar lavage; PMA, phorbol 12-myristate 13-acetate; GM-CSF, granulocyte-macrophage colony-stimulating factor; MCP-1, monocyte chemoattractant protein-1; CCL-3, macrophage inflammatory protein 1-α; TLR, Toll-like receptor.

Acknowledgments

Author Contributions

All authors made a significant contribution to the work reported, whether that is in the conception, study design, execution, acquisition of data, analysis, and interpretation, or in all these areas; took part in drafting, revising, or critically reviewing the article; gave final approval of the version to be published; have agreed on the journal to which the article has been submitted; and agree to be accountable for all aspects of the work.

Disclosure

The authors declare no competing interest in this work.

References

1. Ahmar Rauf M, Nisar M, Abdelhady H, Gavande N, Iyer AK. Nanomedicine approaches to reduce cytokine storms in severe infections. *Drug Discov Today*. 2022;27(11):103355. doi:10.1016/j.drudis.2022.103355

2. Bonaventura A, Vecchié A, Dagna L, et al. Endothelial dysfunction and immunothrombosis as key pathogenic mechanisms in COVID-19. *Nat Rev Immunol*. 2021;21(5):319–329. doi:10.1038/s41577-021-00536-9

3. Laurent P, Yang C, Rendeiro AF, et al. Sensing of SARS-CoV-2 by pDCs and their subsequent production of IFN-I contribute to macrophage-induced cytokine storm during COVID-19. *Sci Immunol*. 2022;7(75):eadd4906. doi:10.1126/sciimmunol.add4906

4. Guan T, Zhou X, Zhou W, Lin H. Regulatory T cell and macrophage crosstalk in acute lung injury: future perspectives. *Cell Death Discov*. 2023;9 (1):9. doi:10.1038/s41420-023-01310-7

5. Lin X, Fu B, Xiong Y, et al. Unconventional secretion of unglycosylated ORF8 is critical for the cytokine storm during SARS-CoV-2 infection. *PLoS Pathog*. 2023;19(1):e1011128. doi:10.1371/journal.ppat.1011128

6. Li W, Xu H, Shao J, et al. Discovery of alantolactone as a natural NLRP3 inhibitor to alleviate NLRP3-driven inflammatory diseases in mice. *Br J Pharmacol*. 2023;20. doi:10.1111/bph.16036

7. Dubyak GR, Miller BA, Pearlman E. Pyroptosis in neutrophils: multimodal integration of inflammasome and regulated cell death signaling pathways. *Immunol Rev*. 2023;19. doi:10.1111/imr.13186

8. Hsu CG, Li W, Sowden M, Chávez CL, Berk BC. Pnpt1 mediates NLRP3 inflammasome activation by MAVS and metabolic reprogramming in macrophages. *Cell Mol Immunol*. 2023;20(2):131–142. doi:10.1038/s41423-022-00962-2

9. Linden J, Koch-Nolte F, Dahl G. Purine release, metabolism, and signaling in the inflammatory response. *Annu Rev Immunol*. 2019;37:325–347. doi:10.1146/annurev-immunol-051116-052406

10. Liu J, Wang L-N. Neurogenic dysphagia in traditional Chinese medicine. *Brain Behav*. 2020;10(11):e01812. doi:10.1002/brb3.1812

11. Torres-Rosas R, Yehia G, Peña G, et al. Dopamine mediates vagal modulation of the immune system by electroacupuncture. *Nat Med*. 2014;20 (3):291–295. doi:10.1038/nm.3479

12. Liu S, Wang Z-F, Su Y-S, et al. Somatotopic organization and intensity dependence in driving distinct NPY-expressing sympathetic pathways by electroacupuncture. *Neuron*. 2020;108(3):436–450.e7. doi:10.1016/j.neuron.2020.07.015

13. Weaver LK, Chu N, Behrens EM. Interferon-γ–mediated immunopathology potentiated by toll-like receptor 9 activation in a murine model of macrophage activation syndrome. *Arthritis Rheumatol*. 2019;71(1):161–168. doi:10.1002/art.40683

14. Shimazu H, Munakata S, Tashiro Y, et al. Pharmacological targeting of plasmin prevents lethality in a murine model of macrophage activation syndrome. *Blood*. 2017;130(1):59–72. doi:10.1182/blood-2016-09-738096

15. Yang L, Ding W, Dong Y, et al. Electroacupuncture attenuates surgical pain-induced delirium-like behavior in mice via remodeling gut microbiota and dendritic spine. *Front Immunol*. 2022;13:955581. doi:10.3389/fimmu.2022.955581

16. Ash MK, Bhimalli PP, Cho BK, et al. Bulk IgG glycosylation predicts COVID-19 severity and vaccine antibody response. *Cell Rep*. 2022;41 (11):111799. doi:10.1016/j.celrep.2022.111799

17. Tang J, Zeng C, Cox TM, et al. Respiratory mucosal immunity against SARS-CoV-2 after mRNA vaccination. *Sci Immunol*. 2022;7(76):eadd4853. doi:10.1126/sciimmunol.add4853

18. Wu J, Lan Y, Shi X, et al. Sennoside A is a novel inhibitor targeting caspase-1. *Food Funct*. 2022;13(19):9782–9795. doi:10.1039/d2fo01730j

19. Behrens EM, Canna SW, Slade K, et al. Repeated TLR9 stimulation results in macrophage activation syndrome-like disease in mice. *J Clin Invest*. 2011;121(6):2264–2277. doi:10.1172/JCI43157

20. Tang S, Yang C, Li S, et al. Genetic and pharmacological targeting of GSDMD ameliorates systemic inflammation in macrophage activation syndrome. *J Autoimmun*. 2022;133:102929. doi:10.1016/j.jaut.2022.102929

21. Liu X, Fan T, Guan J, et al. Dopamine relieves inflammatory responses through the D2 receptor after electroacupuncture at ST36 in a mouse model of chronic obstructive pulmonary disease. *Acupunct Med*. 2023;41(3):163–174. doi:10.1177/09645284221107684

22. Liu XY, Su JC, Zhang XF, et al. Electroacupuncture preconditioning improves pulmonary function via inhibiting inflammatory response and up-regulating expression of ACE2 and Ang (1–7) in lipopolysaccharide-induced acute lung injury rats. *Zhen Ci Yan Jiu*. 2022;47(8):684–689. Chinese. doi:10.13702/j.1000-0607.20210979

23. Huang D, Chen M, Wang Z, Hou L, Yu W. Electroacupuncture pretreatment attenuates inflammatory lung injury after cardiopulmonary bypass by suppressing NLRP3 inflammasome activation in rats. *Inflammation*. 2019;42(3):895–903. doi:10.1007/s10753-018-0944-y

24. Wu Y, Huang D, Wang X, et al. Suppression of NLRP3 inflammasome by Platycodin D via the TLR4/MyD88/NF-κB pathway contributes to attenuation of lipopolysaccharide induced acute lung injury in rats. *Int Immunopharmacol*. 2021;96:107621. doi:10.1016/j.intimp.2021.107621

25. Fajgenbaum DC, June CH. Cytokine Storm. *N Engl J Med*. 2020;383(23):2255–2273. doi:10.1056/NEJMra2026131

26. Chaturvedi V, Marsh RA, Zoref-Lorenz A, et al. T-cell activation profiles distinguish hemophagocytic lymphohistiocytosis and early sepsis. *Blood*. 2021;137(17):2337–2346. doi:10.1182/blood.2020009499

27. Arora H, Wilcox SM, Johnson LA, et al. The ATP-binding cassette gene ABCF1 functions as an E2 ubiquitin-conjugating enzyme controlling macrophage polarization to dampen lethal septic shock. *Immunity*. 2019;50(2):418–431.e6. doi:10.1016/j.immuni.2019.01.014

28. Camilli G, Blagojevic M, Naglik JR, Richardson JP. Programmed cell death: central player in fungal infections. *Trends Cell Biol*. 2021;31 (3):179–196. doi:10.1016/j.tcb.2020.11.005

29. Wang Y, Zhang L, Zhou F. Cuproptosis: a new form of programmed cell death. *Cell Mol Immunol*. 2022;19(8):867–868. doi:10.1038/s41423-022-00866-1

30. Kajarabille N, Latunde-Dada GO. Programmed cell-death by ferroptosis: antioxidants as mitigators. *Int J Mol Sci*. 2019;20(19):4968. doi:10.3390/ijms20194968

31. Savio LEB, Robson SC, Longhi MS. Ectonucleotidase modulation of lymphocyte function in gut and liver. *Front Cell Dev Biol*. 2022;8:621760. doi:10.3389/fcell.2020.621760

32. Fu J, Wu H. Structural mechanisms of NLRP3 inflammasome assembly and activation. *Annu Rev Immunol*. 2023;41:301–316. doi:10.1146/annurev-immunol-081022-021207

33. Elias EE, Lyons B, Muruve DA. Gasdermins and pyroptosis in the kidney. *Nat Rev Nephrol*. 2023. doi:10.1038/s41581-022-00662-0

34. Zhang T, Lu L, Li M, et al. Exosome from BMMSC attenuates cardiopulmonary bypass-induced acute lung injury via YAP/β-catenin pathway: downregulation of pyroptosis. *Stem Cells*. 2022;40(12):1122–1133. doi:10.1093/stmcls/sxac063

35. Lv ZY, Shi YL, Bassi GS, et al. Electroacupuncture at ST36 (Zusanli) prevents T-Cell lymphopenia and improves survival in septic mice. *J Inflamm Res*. 2022;15:2819–2833. doi:10.2147/JIR.S361466

36. Kong JT, Puetz C, Tian L, et al. Effect of electroacupuncture vs sham treatment on change in pain severity among adults with chronic low back pain: a randomized clinical trial. *JAMA Netw Open*. 2020;3(10):e2022787. doi:10.1001/jamanetworkopen.2020.22787

37. Zhou F, Jiang H, Kong N, et al. Electroacupuncture attenuated anxiety and depression-like behavior via inhibition of hippocampal inflammatory response and metabolic disorders in TNBS-induced IBD rats. *Oxid Med Cell Longev*. 2022;2022:8295580. doi:10.1155/2022/8295580

38. Jia YZ, Li HT, Zhang GM, et al. Electroacupuncture alleviates orofacial allodynia and anxiety-like behaviors by regulating synaptic plasticity of the CA1 hippocampal region in a mouse model of trigeminal neuralgia. *Front Mol Neurosci*. 2022;15:979483. doi:10.3389/fnmol.2022.979483

39. Yen CM, Wu TC, Hsieh CL, Huang YW, Lin YW. Distal electroacupuncture at the LI4 acupoint reduces CFA-induced inflammatory pain via the brain TRPV1 signaling pathway. *Int J Mol Sci*. 2019;20(18):4471. doi:10.3390/ijms20184471

40. Xu S, Yu L, Luo X, et al. Manual acupuncture versus sham acupuncture and usual care for prophylaxis of episodic migraine without aura: multicentre, randomised clinical trial. *BMJ*. 2020;368:m697. doi:10.1136/bmj.m697

41. Yu C, Shen F, Kong L, Wang X, Jiang T. Analysis of the current situation of sham acupuncture control in acupuncture animal experiments. *J Tradition Chin Med*. 2019;60:1509–1513. doi:10.13288/j.11-2166/r.2019.17.016